Journal for ImmunoTherapy of Cancer

KLF12 overcomes anti-PD-1 resistance by reducing galectin-1 in cancer cells

Yujia Zheng,[1,2] Hao Zhang,[1] Chu Xiao ,[1] Ziqin Deng,[1] Tao Fan,[1] Bo Zheng,[3] Chunxiang Li,[1] Jie He [1]

To cite: Zheng Y, Zhang H, Xiao C, *et al*. KLF12 overcomes anti-PD-1 resistance by reducing galectin-1 in cancer cells. *Journal for ImmunoTherapy of Cancer* 2023;**11**:e007286. doi:10.1136/jitc-2023-007286

► Additional supplemental material is published online only. To view, please visit the journal online (http://dx.doi.org/10.1136/jitc-2023-007286).

YZ and HZ contributed equally.
CL and JH contributed equally.

Accepted 26 July 2023

[1]Department of Thoracic Surgery, National Cancer Center/National Clinical Research Center for Cancer/Cancer Hospital, Chinese Academy of Medical Sciences and Peking Union Medical College, Beijing, China
[2]Cancer Center, Union Hospital, Tongji Medical College, Huazhong University of Science and Technology, Wuhan, China
[3]Department of Pathology, National Cancer Center/National Clinical Research Center for Cancer/Cancer Hospital, Chinese Academy of Medical Sciences and Peking Union Medical College, Beijing, China

Correspondence to
Dr Jie He; prof_jiehe@yeah.net

Professor Chunxiang Li; lichunxiang@cicams.ac.cn

ABSTRACT

Backgrounds Immune checkpoint blockade has revolutionized cancer treatment and has improved the survival of a subset of patients with cancer. However, numerous patients do not benefit from immunotherapy, and treatment resistance is a major challenge. Krüppel-like factor 12 (KLF12) is a transcriptional inhibitor whose role in tumor immunity is unclear.

Methods We demonstrated a relationship between KLF12 and CD8$^+$ T cells in vivo and in vitro by flow cytometry. The role and underlying mechanism that KLF12 regulates CD8$^+$ T cells were investigated using reverse transcription and quantitative PCR, western blot FACS, chromatin immunoprecipitation-PCR and Dual-Luciferase reporter assays, etc, and employing small interfering RNA (siRNA) and inhibitors. In vivo efficacy studies were conducted with multiple mouse tumor models, employing anti-programmed cell death protein 1 combined with KLF12 or galectin-1 (Gal-1) inhibitor.

Results Here, we found that the expression of tumor KLF12 correlates with immunotherapy resistance. KLF12 suppresses CD8$^+$ T cells infiltration and function in vitro and in vivo. Mechanistically, KLF12 inhibits the expression of Gal-1 by binding with its promoter, thereby improving the infiltration and function of CD8$^+$ T cells, which plays a vital role in cancer immunotherapy.

Conclusions This work identifies a novel pathway regulating CD8$^+$ T-cell intratumoral infiltration, and targeting the KLF12/Gal-1 axis may serve as a novel therapeutic target for patients with immunotherapy resistance.

WHAT IS ALREADY KNOWN ON THIS TOPIC

⇒ Krüppel-like factor 12 (KLF12) is a transcriptional inhibitor that binds to target gene promoters. To date, studies on KLF12 have primarily focused on its role in tumor metastasis and as a sponge for various microRNAs, however, its effect on the tumor microenvironment has not been investigated yet.

WHAT THIS STUDY ADDS

⇒ KLF12 depletion significantly decreased CD8$^+$ T-cell infiltration and inhibited CD8$^+$ T-cell function.

⇒ KLF12 could directly bind to the promoter region of galectin-1 (Gal-1) and inhibit its expression. The primary mechanism by which KLF12 promotes CD8$^+$ T-cell infiltration and function is due to Gal-1 downregulation.

⇒ Decreased KLF12 and increased Gal-1 expression are associated with the resistance to anti-programmed cell death protein 1 (PD-1) immunotherapy, increased KLF12 expression or the combined use of Gal-1 inhibitors can improve anti-PD-1 response.

HOW THIS STUDY MIGHT AFFECT RESEARCH, PRACTICE OR POLICY

⇒ The study highlights the importance of KLF12 depletion and Gal-1 overexpression in immune suppression.

⇒ These findings provide useful mechanistic insights into the antitumor and potential synergistic effects of combining immune checkpoint blockade with a Gal-1 inhibitor in tumors, and the KLF12/Gal-1 axis may serve as a novel therapeutic target.

INTRODUCTION

Checkpoint inhibition immunotherapy, including programmed cell death protein 1 (PD-1), programmed death-ligand 1 (PD-L1), and cytotoxic T lymphocyte antigen 4 blockers, has emerged as one of the most clinically effective strategies for cancer treatment.[1] Immunotherapies targeting immune checkpoint inhibitors (ICIs) have revolutionized the treatment of tumors by revitalizing and boosting T-cell responses. However, most patients with cancer do not respond to immune checkpoint therapy or do not have a durable response.[2 3] In particular, PD-1/PD-L1 blockers are most effective in clinical applications, whereas the average objective response rate across all cancer types is only 20–25%.[4] Combination therapy is a promising approach to overcoming PD-1/PD-L1 resistance and improving the efficacy rate.[5] The type and density of immune cells present in the tumor microenvironment (TME) are predictors of their response to treatment.[6] Different immune cell subsets restrict and influence each other in tumor cells of the TME. Understanding the complex interactions between immune cells and tumor cells in the TME is crucial for elucidating the mechanisms of immune resistance.[7] This is conducive to the discovery of potential targets and combination therapies.[8]

Krüppel-like factor 12 (KLF12) is a transcriptional inhibitor that binds to target gene promoters.[9] To date, studies on KLF12 have primarily focused on its role in tumor metastasis[10] and as a sponge for various microRNAs.[11 12] In cisplatin-resistant ovarian cancer cells, KLF12 is reported to be recruited to the ISG15 promoter region and repressed the transcriptional activation of ISG15.[13] In colorectal cancer, EGR1 is also a direct target of KLF12 and overexpression of EGR1 promoted cell growth in vitro and tumor growth.[14] Our previous studies have shown that KLF12 affects tumor angiogenesis,[15] however, its effect on the TME has not been investigated yet. To determine the effect of KLF12 on the TME, we established mouse models using KLF12 knockout and overexpressed cell lines. These results indicated that KLF12 depletion significantly decreased $CD8^+$ T-cell infiltration and inhibited $CD8^+$ T-cell function.

Galectin-1 (Gal-1) belongs to the family of endogenous glycan-binding proteins that have crucial roles in tumor aggressiveness and progression of tumors.[16 17] It can directly bind to a variety of glycosylated ligands on the surface of immune cells, stromal cells and tumor cells.[18] Gal-1 is an immune regulatory molecule functioning in tumor immunity.[19] Gal-1 inhibits T-cell activation and induces T-cell apoptosis[20 21] and functions in promoting T cell-dependent immune escape, such as inhibiting the secretion of anti-inflammatory factors[22] and reducing T-cell infiltration.[23] Accumulating evidence shows that dysregulated expression of Gal-1 in TME contributes to the immunosuppression via its binding to T-cell surface glycosylated receptors that modulate effector function.[24 25] Blocking this inhibitory signal can enhance the immune response against tumor cells, which has profound implications in cancer immunotherapy.[20 23 26] However, the extensive regulatory mechanisms of Gal-1 in multiple tumor tissues remain unclear.

In the current study, we aimed to explore the molecular mechanisms of malignancy and immunotherapy resistance related to KLF12 that may provide insights into predicting anti-PD-1 responses and new drug development. The results of chromatin immunoprecipitation sequencing (ChIP-seq) and transcriptomic sequencing and dual fluorescence report experiments suggested that KLF12 could directly bind to the promoter region of Gal-1 and inhibit its transcription. The primary mechanism by which KLF12 promotes $CD8^+$ T-cell infiltration is due to Gal-1 downregulation. Indeed, our results indicate that KLF12 and Gal-1 can predict the therapeutic effect of anti-PD-1, and targeted KLF12/Gal-1 therapy transforms a T cell-desolate tumor into one enriched for T cells and consequently increases sensitivity to anti-PD-1 therapy.

MATERIALS AND METHODS

Mice

Wild-type C57BL/6 and nude mice were purchased from Beijing HFK Bioscience, China. OT-1 mice with a C57BL/6 background were obtained from Shanghai Model Organisms. Study protocols involving mice were approved by the Institutional Animal Care and Use Committee at National Cancer Center/Cancer Hospital, Chinese Academy of Medical Sciences & Peking Union Medical College. The mice were maintained under specific pathogen-free conditions, and food and water were provided ad libitum. All animals were examined before the initiation of the study to ensure that they were healthy and acclimated to the laboratory environment. The maximum tumor size was ≤2000 mm^3.

A549 (1.0×10^6), H322 (1.0×10^6), LLC (3.0×10^5), MC-38 (5.0×10^5), and B16-F10 (3.0×10^5) cells were subcutaneously injected into nude mice. Tumor volume was monitored dynamically. On Days 5 and 10, DiR iodide (Yeasen)-labeled OT-1 $CD8^+$ T cells (1.0×10^6) were injected intravenously into LLC and B16-F10 tumor-bearing mice.

LLC (3.0×10^5), MC-38 (5.0×10^5), and B16-F10 (3.0×10^5) cells were subcutaneously injected into C57BL/6 mice and used for flow cytometry or treatment experiments (with inhibitor and monoclonal antibodies). Five days after tumor cell inoculation, anti-human Gal-1 inhibitor (5 mg/kg, HY-19756, MCE), PD-1 (250 µg per mouse, clone Rmp1-14, BE0146, Bio X Cell), or immunoglobulin G (IgG, 250 µg per mouse, clone MOPC-21, BE0083, Bio X Cell) were intraperitoneally injected on alternative day.

In the survival analysis, a mouse tumor with a maximum diameter of 2.0 cm was considered dead. All experiments included at least five mice per group.

IncuCyte cell proliferation and wound healing assays

Incucyte living cell imaging enables non-invasive, complete kinetic measurement of cell growth based on area (confluence) measurements. Cells (3×10^3) were inoculated into 96-well plates and cell proliferation was evaluated based on the degree of cell fusion. Cells of 8×10^4 cells were seeded in 96-well plates and grown to 90% confluence. IncuCyte ZOOM was used to create the wounds. Cells were imaged every 12 hours using an IncuCyte (Essen BioScience, USA).

In vitro transendothelial migration assays

HUVEC and C166 were cultured with tumor cell conditioned medium (CM) for 24 hours. Next, 5000 live cells each were seeded on a Transwell insert that was precoated with matrigel matrix (Corning). Equal numbers of peripheral blood mononuclear cells (PBMCs) or splenic T cells (2×10^5 to 3×10^5) were added to the upper chamber of each Transwell in serum-free medium. The lower chamber was filled with CM. After a 24-hour incubation at 37°C, media in the lower chamber were collected, and the number of cells that migrated were counted with a hemocytometer.

Flow cytometry

Live/dead cell discrimination was performed using the Zombie Yellow Fixable Viability Kit (BioLegend). Cell surface staining was performed for 30 min at 4°C. The cells

were fixed with 4% paraformaldehyde for 30 min at 4°C, permeabilized with the permeabilization buffer, followed by staining with granzyme B (GZMB), interferon (IFN)-γ, and tumor necrosis factor (TNF)-α antibodies for 60 min at 4°C. Details of the antibodies were summarized in additional file: online supplemental table S1.

BrdU assay

$CD8^+$T cells (1×10^6/well) from diverse groups were cultivated within the 24-well plates under 37°C and 5% CO2 conditions for a 12 hours period. Thereafter, all wells were added with 10 µM of Brdu (MCE) to achieve 60–120 min cell incubation. Wash cells in Cell Staining Buffer, and then 4% paraformaldehyde at room temperature for 20–30 min, 15 min 0.5% Triton X-100 treatment, and another 1-hour incubation using Dulbecco's phosphate-buffered saline (DPBS) with 20 µg of DNAse. Cells were later incubated with anti-BrdU antibody (BioLegend) for a 20 min. 4',6-Diamidino-2-phenylindole dihydrochloride (DAPI) was adopted for cell nuclear staining.

RNA isolation, reverse transcription, and quantitative RT-PCR

Total RNA was extracted using an RNA Extraction Kit (Yishan Biotechnology) and reverse-transcribed using the Reverse Transcription System (Takara), according to the manufacturer's protocol. Complementary DNA (cDNA) was analyzed by quantitative PCR (qPCR) using SYBR Green PCR Master Mix (Takara), which was performed on an applied biosystems (ABI) real-time PCR detection system. The experimental results were normalized to those for glyceraldehyde-3-phosphate dehydrogenase (GAPDH). All the primer sequences are listed in additional file: online supplemental table S2.

RNA sequencing and analysis

Total RNA was extracted according to the manufacturer's instructions. RNA integrity was assessed using an RNA Nano 6000 Assay Kit on the Bioanalyzer 2100 system (Agilent Technologies, California, USA). cDNA library preparation and RNA sequencing (RNA-seq) were performed using Novogene (Beijing, China). Briefly, messenger RNA (mRNA) was randomly fragmented in a fragmentation buffer and reverse-transcribed into cDNA. The cDNA library was sequenced on an Illumina platform and 150 bp paired-end reads were generated. RNA-seq read quality was evaluated using FastQC, followed by establishing the index of the reference genome and aligning the clean paired-end reads to the reference genome using HISAT2. Differential expression analysis was performed using DESeq2. Genes with an adjusted p value<0.05 were assigned as differentially expressed. The differentially expressed genes (DEGs) of A549 and KYSE30 was listed in additional file: online supplemental tables 4,5.

Data source and analysis

RNA-seq data (fragments per kilobase of exon per million) and corresponding clinical information of patients with cancer were obtained from the The Cancer Genome Atlas (TCGA) database (https://portal.gdc.cancer.gov/). Kaplan-Meier analyses of overall survival were performed using the R package survminer version (https://cran.r-project.org/web/packages/survminer/index.html). Pearson correlation analysis was performed to determine the correlations between classical immune checkpoints using the corrplot and ggplot2 R packages.

Transient transfection and lentivirus preparation

When cell lines were at 50% confluence, siRNAs were mixed with Lipofectamine 3000 reagent (Invitrogen) and added to the cell culture, according to the manufacturer's instructions.

HEK293 cells were transfected with a specific gene or shRNA lentiviral expression vector and packaging plasmids (pCMV-VSV-G and psPAX2) using Lipofectamine 3000 (Invitrogen). Lentivirus-containing medium was obtained at 48 and 72 hours after transfection.

CRISPR/dCas9-mediated editing system

The CRISPR/dCas9-mediated editing system was packaged into lentiviruses in HEK293 cells. Thereafter, we conducted KYSE30 and B16-F10 cell lentiviral infection assays using the above methods. Isolation of a single clone from a living part using limited dilution was performed.

ChIP-seq data analysis

ChIP-seq data for GFP-tagged KLF12 in HEK293 cells were downloaded from the NCBI GEO DataSet (GSM2026901).[27] To analyze the ChIP-seq data generated from HepG2 cells, bigwig files were downloaded (GSE170637). The peaks in both data sets were visualized by the nearest gene using the WashU Epigenome Browser (http://epigenomegateway.wustl.edu/browser/).[28 29]

ChIP assay

Cells growing in 15 cm dishes were used for ChIP experiments with the SimpleChIP Enzymatic Chromatin IP Kit (Magnetic Beads, CST#9003). The experiment was performed according to the manufacturer's instructions with a few modifications. Briefly, formaldehyde (final concentration, 1%) was added to fix the cells to 80% confluence (approximately 5×10^6 cells). Glycine (final concentration, 1×) was added to terminate fixation. Thereafter, cells were scraped after adding protease inhibitor cocktail diluted in phosphate buffered saline (final concentration, 1×) and were centrifuged at 2000×g for 5 min at 4°C. After pellet nuclei were centrifuged and resuspended, micrococcal nuclease was added to tubes to digest chromatin for 20 min at 37°C. Diluted chromatin (10 µL) was removed as 2% input samples. The immunoprecipitating antibodies included Flag (CST, 14793S), a positive control antibody against histone H3, and a negative control antibody against normal rabbit IgG. The antibodies were diluted to the recommended concentrations described in the antibody manuals or empirical concentrations. Samples were incubated with antibodies overnight at 4°C with rotation. Protein G Magnetic Beads were added to each sample reaction and incubated, followed

by precipitation and washing of the beads on a magnetic separation rack. Chromatin was eluted using an elution buffer from the beads for 30 min at 65°C. Subsequently, NaCl and proteinase K were added, and the mixture was incubated for 2 hours at 65°C. DNA purification was performed using spin columns, as described in the kit instructions. Purified DNA samples were directly used for DNA library construction for downstream sequencing on Illumina platforms.

Western blotting

Cells were grown in 6 mm dishes. After the cells reached 90% confluence, they were lysed in 250 µL of radioimmunoprecipitation assay (RIPA) buffer (Thermo, 89900) supplemented with protease and phosphatase inhibitors (Thermo, 78442) and centrifuged at 14,000 rpm/min for 30 min at 4°C. The supernatant was stored, and protein concentrations were quantified using the bicinchoninic acid assay (BCA) (Thermo, 23225).

Proteins from each sample were separated using SDS-PAGE and transferred onto polyvinylidene fluoride (PVDF) membranes (Millipore, ISEQ85R). After blocking, primary antibodies against Gal-1 (CST, 12936, 1:1000), KLF12 (Abcam, ab129459, 1:1000), and β-actin (CST, 3700s, 1:1000) were used. After rinsing, the membranes were incubated in horseradish peroxidase (HRP)-linked secondary anti-mouse IgG (CST, 7076, 1:3000) and anti-rabbit IgG antibody (CST, 7074, 1:3000) for 1 hour at room temperature and washed. Finally, protein bands were imaged.

Immunohistochemistry

The tissues were fixed in 10% paraformaldehyde and embedded in paraffin. After continuous sectioning to 6 µm thickness using a microtome, sections were placed on slides and stored at 4°C.

For immunohistochemistry (IHC) staining, the sections were sequentially immersed in xylene, ethanol, and water washers for deparaffinization and rehydration. The sections were boiled in an antigen retrieval buffer and subsequently cooled naturally to room temperature. Sections were blocked and incubated with primary antibodies against Gal-1 (CST, 13888), KLF12 (Bioss, bs-16783R), PD-1 (CST, 84651S), PD-1 (CST, 86163), CD8 (Abcam, 217344), and CD8 (CST, 85336) overnight at 4°C. The following day, the sections were covered with secondary antibody solutions. An appropriate amount of freshly prepared diaminobenzidine (DAB) solution was added to the sections and monitored under a microscope for 1–10 min. Counterstain sections were stained with hematoxylin.

OT-1 T-cell cytotoxicity assays

For the OT-1 T-cell cytotoxicity assays, OVA-B16, OVA-KLF12^{OE}-B16, OVA-B16-F10, and OVA-KLF12^{OE}-B16-F10 were labeled with 1 mM or 0.5 mM 5- or 6-(N-succinimidyloxycarbonyl)-3',6'-O,O'-diacetylfluorescein (CFSE) (Sigma, 21888) in serum-free medium for 15 min at 37°C. The tumor cells were then washed thrice with D 10% fetal bovine serum complete medium. OT-1 T cells were added at different ratios to tumor cells (1×10^5) and incubated for 5–6 hours at 37°C. The cells were collected, stained with propidium iodide (PI), and monitored using flow cytometry.

Luciferase reporter assays

HEK293T cells seeded in 12-well plates, were transiently transfected with the LGALS1 promoter or the indicated mutant, along with the pCDH-KLF12 and Renilla Luciferase reporter. Luciferase assays were subsequently performed 48 hours after transfection using the Dual-Luciferase Reporter Assay System protocol (Promega). Relative luciferase activity was normalized to Renilla Luciferase activity.

Multiplex immunofluorescence

Whole-tissue section slides were de-paraffinized and subjected to antigen retrieval using EDTA buffer (Sigma-Aldrich) pH=8.0 and boiled for 1 hour at 96°C in a pressure-boiling container (PT Module, Lab Vision). The sections were blocked for 10 min at room temperature. The sections were incubated with primary antibodies against Gal-1 (CST, 13888), KLF12 (Bioss, bs-16783R), PD-1 (CST, 84651S), PD-1 (CST, 86163), CD8 (Abcam, 217344), and CD8 (CST, 85336) for 1 hour at room temperature. Staining was performed consecutively, and each marker was detected before the application of the next antibody. According to the manufacturer's instructions, the primary antibody was detected using the Opal Polymer HRP Ms$^+$ Rb detection reagent, and Opal 5-Color Manual IHC was performed with four reactive fluorophores: Opal 520, Opal 570, Opal 620, and Opal 650 plus DAPI nuclear counterstain (Panovue, PerkinElmer).

Patient cohort and evaluation of treatment response

We collected 161 non-small cell lung cancer (NSCLC), 53 esophageal, and 173 colorectal cancer (online supplemental table S3) tissue samples from the biobank of the National Cancer Center/National Cancer/Tumor Hospital, the Chinese Academy of Medical Sciences, and the Peking Union Medical College (Beijing, China). All patients received standard treatment after surgery.

Twenty with NSCLC and 46 with esophageal cancer (online supplemental table S3) were treated with anti-PD-1, and their response was evaluated according to the solid tumor response evaluation criteria (RECIST) V.1.1.[30]

Statistical analysis

Statistical analyses were performed with GraphPad Prism software V.8 using the Student's t-test, Kaplan-Meier method, and log-rank (Mantel-Cox) test. Data are represented as the mean±SD from at least three independent experiments. *P value<0.05 and **p value<0.01 were considered statistically significant.

RESULTS

Tumor KLF12 is critical for intrinsic resistance to tumor immunity

We have previously shown that KLF12 expression level correlates with angiogenesis.[15] To further elucidate the function of KLF12, we analyzed data from TCGA and confirmed that KLF12 expression was higher in normal tissues than that in tumor tissues (online supplemental figure S1A). Furthermore, KLF12 mRNA expression positively correlated with overall survival in multiple tumors (online supplemental figure S1B,C). Therefore, we investigated the prognostic value of KLF12 in 161 NSCLC, 53 esophageal cancers, and 173 colorectal cancers. We found that the expression of KLF12 was significantly decreased in tumors (figure 1A–C). High KLF12 expression favored better patient survival (figure 1A–C). In addition, we observed a significant association between KLF12 expression and lymph node metastasis, as well as clinical stage (figure 1D and online supplemental figure S1D).

Additionally, we established KLF12-transfected cell lines and inoculated them into nude and C57BL/6J mice. Both in vivo and in vitro experiments showed that KLF12 expression did not affect the growth of human lung and esophageal cancer cell lines (figure 1E,F, and online supplemental figure S2B–D). Moreover, wound healing assays demonstrated that cancer cells overexpressing KLF12 inhibited cell migration and KLF12 depletion promoted cell migration compared with control cells (online supplemental figure S2A). To validate these results, we performed experiments using mouse cell lines. Notably, KLF12-knockdown LLC and KLF12-knockout B16-F10 had no effect on tumor growth in nude mice (immune-deficient) (figure 1G,I and online supplemental figure S2E,G); whereas it accelerated tumor progression in C57BL/6J (immune-competent) mice (figure 1H,J, and online supplemental figure S2F,H). Thus, ectopically expressed KLF12 resulted in slower MC38 tumor progression in C57BL/6J mice (figure 1K and online supplemental figure S2I) and comparable tumor progression in nude mice (figure 1L and online supplemental figure S2J). These results suggested that KLF12 may act synergistically with tumor immune cells.

Tumor KLF12 increases CD8$^+$ T-cell infiltration

We analyzed the relationship between KLF12 and immune cell infiltration and found that KLF12 positively correlated with immune cell infiltration in TCGA (online supplemental figure S3A). To determine the mechanism by which tumor KLF12 promotes tumor progression by regulating the TME, we identified the differences in the infiltration of immune cells (CD4, CD8, natural killer (NK), natural killer T cells (NKT), M1, M2, and myeloid-derived suppressor cell (MDSC)). By analyzing the proportion of immune cell invasion in the TME, spleen, and drained lymph nodes (TdLNs), we found significantly decreased infiltration of CD8$^+$ T cells in KLF12^{SH} LLC (figure 2A top and online supplemental figure S3B,C left) and KLF12^{KO} B16-F10 tumors (figure 2A middle, and online supplemental figure S3B,C middle) and increased infiltration of CD8$^+$ T cells in KLF12^{OE} MC38 tumors (figure 2A bottom and online supplemental figure S3B,C right). These conclusions were verified via IHC analysis, and the results showed that KLF12 depletion reduced intratumoral CD8$^+$ infiltration compared with the control in the LLC tumor model (figure 2B, top). Similar results were obtained in B16-F10 melanoma models with KLF12 knockout (figure 2B, middle panel). Conversely, CD8$^+$ T-cell infiltration in the TME increased significantly following KLF12 overexpression (figure 2B, bottom). To investigate the role of CD8$^+$ T cells in cancer progression, we established OVA-B16-F10, OVA-KLF12^{KO}-B16-F10, OVA-LLC, and OVA-KLF12^{SH}-LLC tumors in nude mice. After 5 days, OT-1 CD8$^+$ T cells were intravenously transferred into these mice. We found no difference in tumor volume between the control and KLF12 depletion groups without CD8$^+$ T-cell injection; whereas significant differences were observed in the groups with OT-1 CD8$^+$ T-cell injection (figure 2C,D top and online supplemental figure S3D,E). Fluorescence signal and immunohistochemical results were found that transferred CD8$^+$ T cells decreased in KLF12 knockout and knockdown tumors (figure 2C,D bottom). For further analysis, C57BL/6J mice following CD8 deletion were subcutaneously implanted with wild-type (WT) and KLF12^{KO} B16-F10 cells, and the tumor growth difference between the two groups was significantly reduced (figure 2E and online supplemental figure S3F). These results indicated that KLF12 induces CD8$^+$ T-cell infiltration in the TME. In the in vitro transendothelial migration assays, we observed a decrease in the number of migrating T cells in KLF12 depletion CM compared with that in WT CM (figure 2F), and an increase of CD8$^+$ T cell

infiltration in KLF12^{OE} CM (figure 2F). To extend this observation, we performed identical experiments on human lung and esophageal cancer cell lines and obtained similar results (figure 2G). Collectively, these results suggested that tumor KLF12 can induce CD8$^+$ T-cell accumulation at the tumor site.

Tumor KLF12 suppresses antitumor CD8$^+$ T-cell responses

Next, we investigated the functions of CD8$^+$ T cells isolated from the tumor tissues of MC38 and B16-F10 tumor-bearing mice. Flow cytometry analysis revealed that the production of IFN-γ, TNF-α, and GZMB was higher, and that of annexin V was lower in KLF12^{OE} MC38 tumor tissues (figure 3A), tumor-draining lymph nodes (figure 3B), and spleen (online supplemental figure S4A) than in those with WT MC38 tumors. To validate these results, we investigated the WT and KLF12^{KO} B16-F10 tumors. We found that the level of IFN-γ$^+$, TNF-α$^+$, and GZMB$^+$ CD8$^+$ T cells were lower, and that of annexin V (figure 3E) was higher in KLF12^{KO} B16-F10 tumor tissues (figure 3C) and TdLNs (figure 3D) than that in WT B16-F10 tumors. Next, we examined whether KLF12 knockout cells directly inhibited CD8$^+$ T-cell activation in vitro. We used the CM from WT and KLF12^{KO} B16-F10 tumor cells

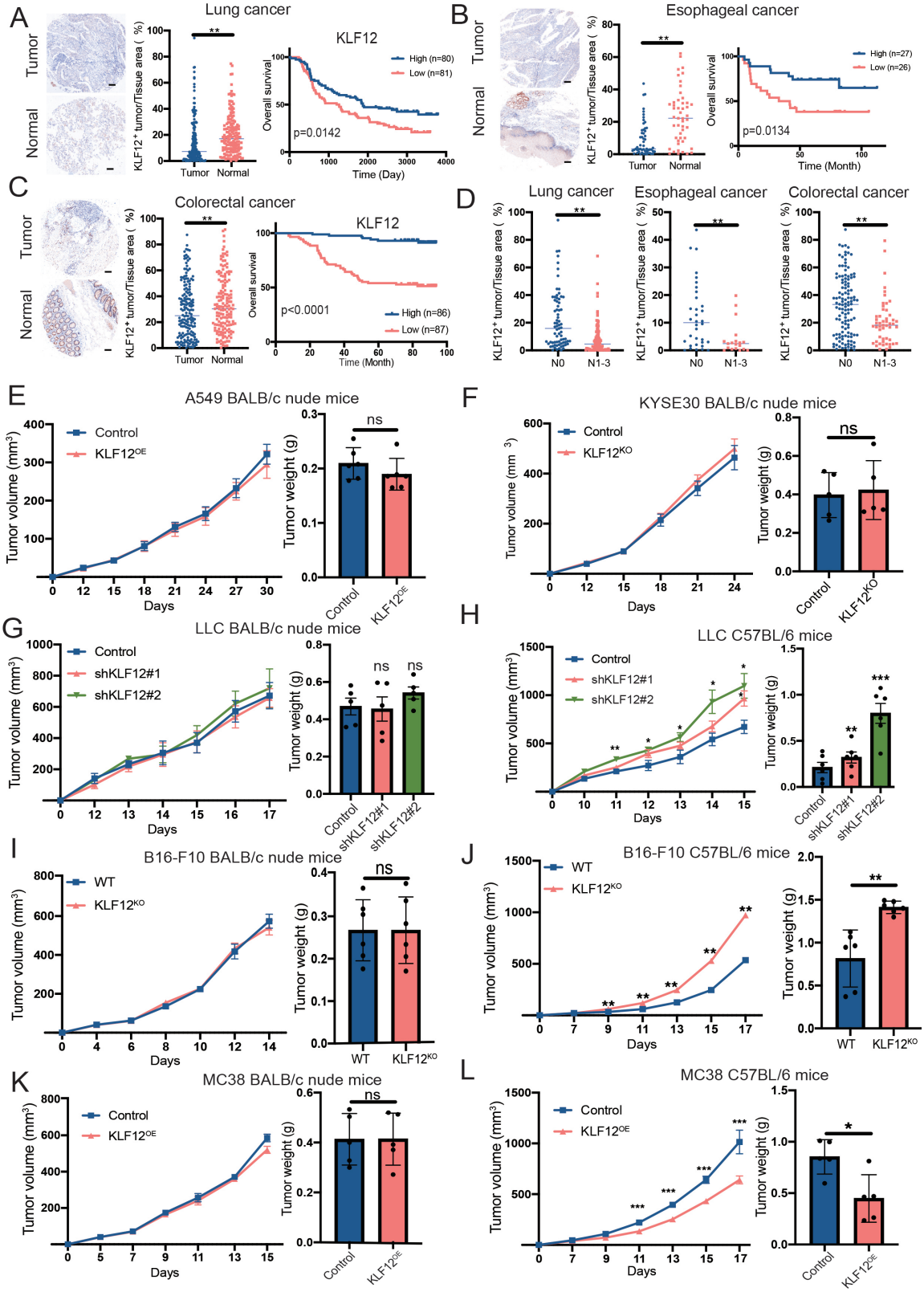

Figure 1 Tumor KLF12 is essential for intrinsic resistance to tumor immunity. (A–C) Immunohistochemistry staining of human tumor tissues and paired adjacent normal tissues. Scale bars, 100 µm. KLF12 expression in lung, esophageal, and colorectal cancer and its relationship with prognosis. (D) Comparison of KLF12 expression among patients with different N staging. (E) Tumor growth curves, tumor weight of control, and KLF12^{OE} A549 cells in nude mice. (F) Tumor growth curves and tumor weight of wild-type (WT) and KLF12^{KO} KYSE30 cells in nude mice. (G–H) Tumor growth curves and weight of control LLC and KLF12^{SH} LLC cells in nude (G) and C57BL/6J mice (H). (I–J) Tumor growth curves and weight of WT and KLF12^{KO} B16-F10 cells in nude (I) and C57BL/6J mice (J). (K–L) Tumor growth curves and weight of control and KLF12^{OE} MC38 cells in nude (K) and C57BL/6J mice (L). KLF12, Krüppel-like factor 12.

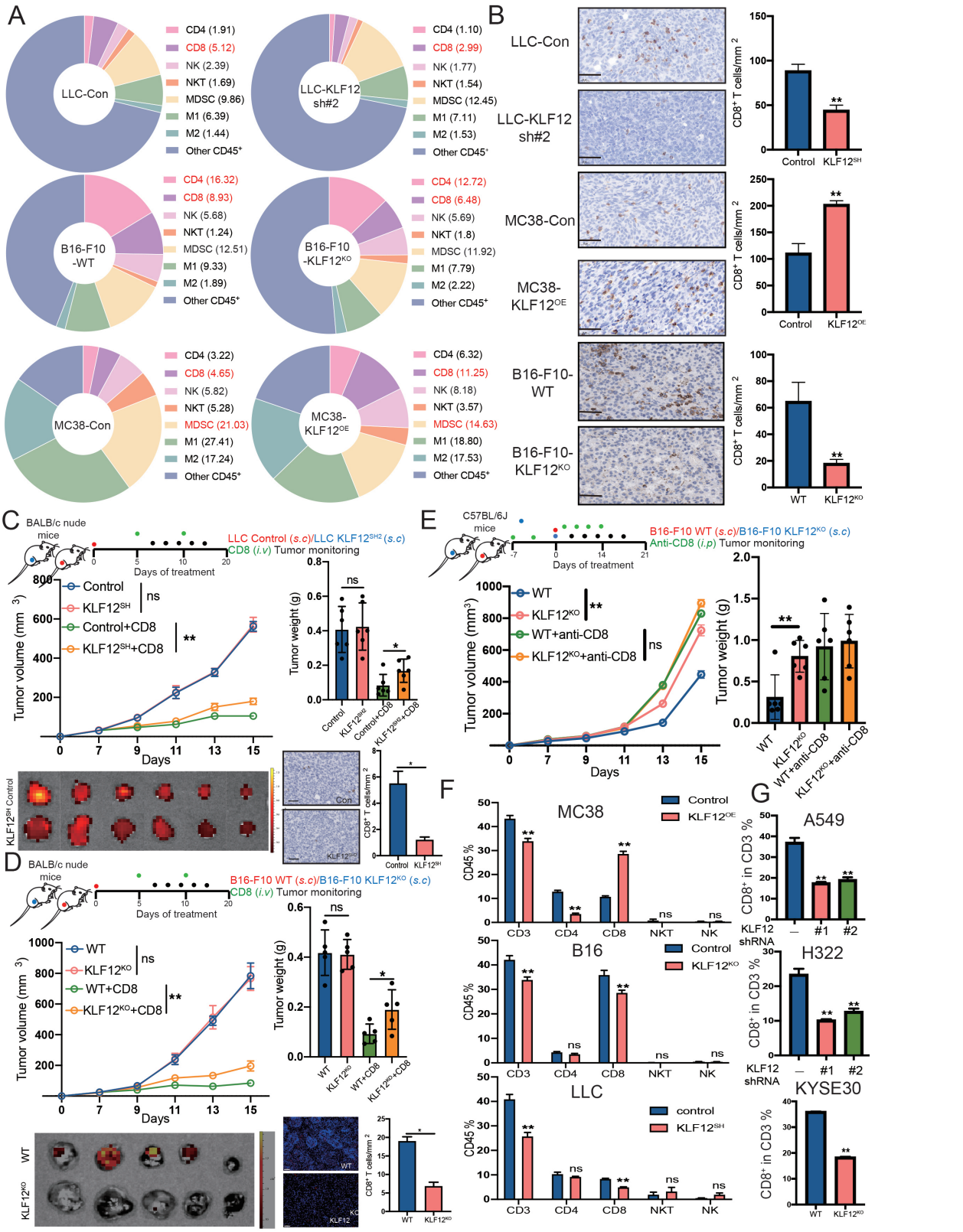

Figure 2 Tumor KLF12 promotes CD8$^+$ T-cell recruitment. (A) Proportions of immune cells among total CD45$^+$ cells were measured using flow cytometry. (B) CD8 was analyzed via immunohistochemistry (IHC) staining (scale bar, 50 µm). (C, D) OVA-LLC and OVA-shKLF12-LLC, OVA-B16-F10 and OVA-KLF12^{KO} B16-F10 tumor-bearing mice initially transfused intravenously with DiR-labeled OT-1 CD8$^+$ T cells. CD8 was detected using IHC (scale bar, 50 µm). (E) WT and KLF12^{KO} B16-F10-bearing (s.c.) mice received anti-CD8 or isotype control antibody. (F, G) T-cell migration was quantified via flow cytometry. Migrated cells at the bottom of the well were quantified 24 hours later. LLC, B16-F10, and MC38 CM (F); A549, H322, and KYSE30 CM (G). i.p., intraperitoneally; i.v., intravenous; KLF12, Krüppel-like factor; MDSC. myeloid-derived suppressor cell; NK, natural killer; NKT, natural killer T cell; s.c., subcutaneous; WT, wild-type.

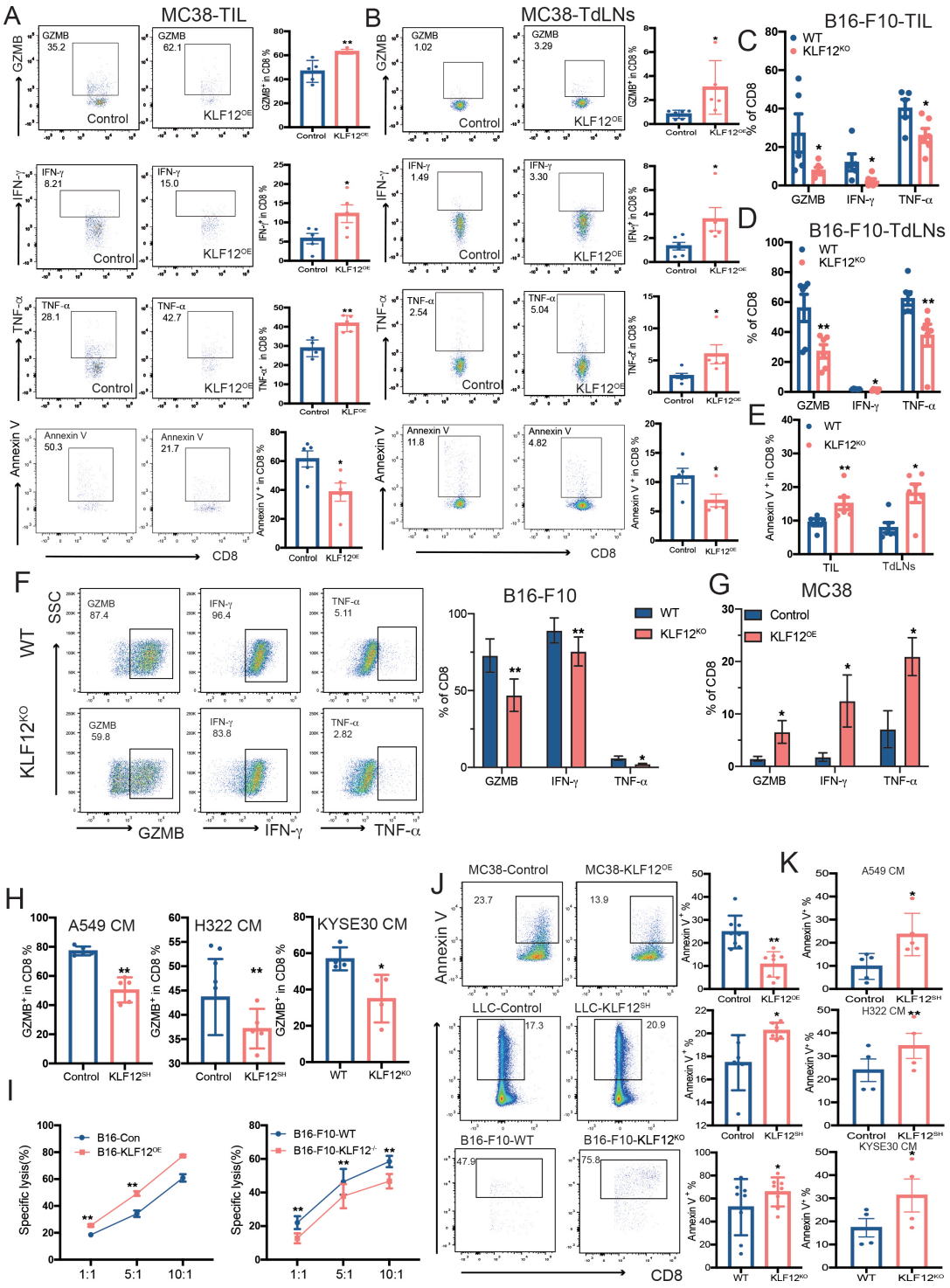

Figure 3 Tumor KLF12 enhances antitumor CD8$^+$ T-cell responses. (A, B) Percentages of GZMB$^+$, IFN-γ$^+$, TNF-α$^+$, annexin V$^+$ CD8$^+$ T cells in TILs (A) and TdLNs (B) bearing KLF12^{OE} and control MC38 tumors detected using flow cytometry. (C, D) Quantification of GZMB, IFN-γ, and TNF-α expression among CD8$^+$ TILs (C) and TdLNs (D) bearing WT and KLF12^{KO} B16-F10 tumors detected by FACS. (E) Percentage of annexin V$^+$ CD8$^+$ in TILs and TdLNs in B16-F10 tumors. (F) Representative flow plot and quantification of GZMB, IFN-γ, and TNF-α expression among CD8$^+$ cells. The CD8 cells were cultured in CM with WT B16-F10 and KLF12^{KO} B16-F10 cells. (G) CD8 cells were cultured in CM with MC38 cells and KLF12^{OE} MC38 cells for 24 hours, and GZMB, IFN-γ, and TNF-α expression was determined using FACS. (H) GZMB expression in CD8$^+$ cells after co-incubation in A549, H322, and KYSE30 CM. (I) Analysis of specific lysis of tumor cells. OVA-B16 tumor and OVA-KLF12^{OE} B16, OVA-B16-F10 tumor and OVA-KLF12^{KO} B16-F10 cells were incubated with OT-1 CD8 T cells at different effectors to target (E:T) ratios (1:1, 5:1, and 10:1) for 4–6 hours, and lysis of tumor cells was analyzed using flow cytometry. (J–K) CD8$^+$ cells were examined for annexin V binding. CM, conditioned medium; FACS, flow cytometry; GZMB, granzyme B; IFN, interferon; KLF12, Krüppel-like factor 12; TdLNs, drained lymph nodes; TIL, tumor-infiltrating lymphocyte; TNF, tumor necrosis factor; WT, wild-type.

after 24 hours to culture CD8 T cells from the spleen of healthy mice. $CD8^+$ T cells showed decreased IFN-γ, TNF-α, and GZMB expression when cultured in KLF12-knockout B16-F10 CM (figure 3F). $CD8^+$ T cells showed higher levels of IFN-γ, TNF-α, and GZMB in the presence of the supernatants from $KLF12^{OE}$ MC38 cells than control cells (figure 3G). To investigate whether reduced KLF12 expression in lung and esophageal cancer cells can induce $CD8^+$ T-cell dysfunction, peripheral blood mononuclear cells isolated from healthy donors were cultured in vitro in the presence of CM. The results showed that GZMB expression in $CD8^+$ T cells decreased in tumor cells with KLF12 depletion (figure 3H), similar to other immune cells (CD4, NK, NKT) (online supplemental figure S4B). We used cells expressing OVA antigen as the target cells to determine whether KLF12 can directly affect the killing ability of T cells. The OVA-B16 and OVA-$KLF12^{OE}$ B16, OVA-B16-F10 and OVA $KLF12^{KO}$ B16-F10 cells were incubated with OT-1 $CD8^+$T cells. Our results showed that OT-1 $CD8^+$ T cells had a more potent cytotoxic effect against tumor cells with high KLF12 expression (figure 3I). CD8 T-cell apoptosis is also an important factor for the low frequency of tumor-infiltrating $CD8^+$ T cells. Thus, we analyzed the apoptosis of $CD8^+$ T cells using annexin V staining. $CD8^+$ T cells cultured in $KLF12^{KO}$ CM were more prone to apoptosis than those cultured with the CM of WT cells. In contrast, $CD8^+$ T cells cultured with $KLF12^{OE}$ MC38 CM showed a lower apoptosis rate (figure 3J). Similar results were observed in human lung and esophageal cancer cell lines (figure 3K). These results confirmed that decreased KLF12 promotes tumor growth in a $CD8^+$ T cell-dependent manner.

KLF12 inhibits Gal-1 transcription by binding to its promoter

To understand the molecular basis of tumor KLF12 regulation in the TME, A549 and KYSE30 cells after KLF12 deletion were subjected to RNA-seq. We identified multiple dysregulated genes in A549 and KYSE30 cells following KLF12 depletion (figure 4A). To identify genes regulated by KLF12 in mice, we analyzed the mouse database GSE166054 for KLF12 overexpression. The heat map shows the DEGs after KLF12 overexpression in mice (figure 4A, right). Integrated analysis of these three RNA-seq data sets revealed that Gal-1 is controlled by KLF12 (figure 4B). Gal-1 is a secreted protein that plays a role in the TME mainly through secreted cells. To further investigate the characteristics of the identified DEGs, we used Kyoto Encyclopedia of Genes and Genomes (KEGG) pathway enrichment methods. We observed that the DEGs were primarily involved in tumor immune regulation, such as cytokine–cytokine receptor interactions and leukocyte transendothelial migration (online supplemental figure S5A).

Next, qPCR and western blotting verified that Gal-1 expression increased when KLF12 decreased, it was significantly inhibited when KLF12 increased (figure 4C,D and online supplemental figure S5B,C). Genome-wide transcription factor binding site data analysis from published ChIP-seq data in HEK293 and HepG2 cells and DNA binding site prediction revealed putative KLF12 binding sites in the Gal-1 promoter (figure 4E). To investigate whether KLF12 physically binds to the promoter region of Gal-1, ChIP and Dual-Luciferase reporter assays were performed. ChIP results showed that KLF12 was recruited to the promoter region of Gal-1 (figure 4F). Luciferase site deletion assay indicated that KLF12 binds to the Gal-1 promoter (figure 4G). To identify the KLF12 domain that interacts with Gal-1, we overexpressed Flag-tagged WT or various truncated KLF12 mutants in HEK293 cells. qPCR revealed that the KLF12 Δ 1–100 mutant impaired Gal-1 suppression (figure 4H). Gal-1 promotes tumor angiogenesis,[31] inhibits T-cell function,[32] and promotes immune resistance.[23] We further investigated Gal-1 and CD8 expression in mouse tumor tissues and their correlation with KLF12 expression. Immunofluorescence was used to detect Gal-1 and CD8 expression in WT LLC and $KLF12^{SH}$ LLC B16-F10 tumors. The results showed that KLF12 expression was negatively correlated with Gal-1 expression and strongly positively correlated with CD8 expression (figure 4I). Similar results were observed in B16-F10 tumors (figure 4J). In MC38 tumors, Gal-1 expression decreased significantly in the KLF12 overexpression group compared with that in the control group, whereas $CD8^+$ T cells infiltration increased significantly (figure 4K). We also identified the relationship between Gal-1 and immune cell infiltration in TCGA and that Gal-1 negatively correlated with immune cell infiltration in most tumors (online supplemental figure S5D). Correlation analysis showed that Gal-1 expression was negatively correlated with $CD8^+$ T-cell infiltration in mouse lung cancer, colorectal cancer, and melanoma (figure 4L). These data suggest that tumor KLF12 downregulates Gal-1 expression in tumors.

Gal-1 is involved in antitumor T-cell regulation

We analyzed the proportion of immune cells in tumors and found that several cells showed high correlation between immune infiltration and Gal-1 expression, and negative correlation between Gal-1 and $CD8^+$ T cells. We further investigated whether the positive effects of tumor KLF12 on T-cell function and infiltration were due to the inhibition of Gal-1. Our experiments demonstrated a negative role of tumor Gal-1 in T-cell function. In vitro transendothelial migration assays, we discovered that Gal-1 silencing abrogated $CD8^+$ T-cell infiltration caused by KLF12 in B16-F10 (figure 5A) and LLC cells (figure 5B). Next, we assessed the effect of OTX008, the inhibitor of Gal-1.[33] $CD8^+$ T-cell infiltration increased significantly after the depletion of KLF12 in H322, A549, KYSE30, LLC and B16-F10 cells by the addition of Gal-1 inhibitor compared with that in the control group (online supplemental figure S6A–C). Flow cytometry analysis showed that KLF12 depletion enhanced the percentage of annexin V^+ $CD8^+$ T cells, which was further inhibited by Gal-1 silencing or inhibitor combination therapy in B16-F10 and LLC cells (figure 5C,D and online supplemental

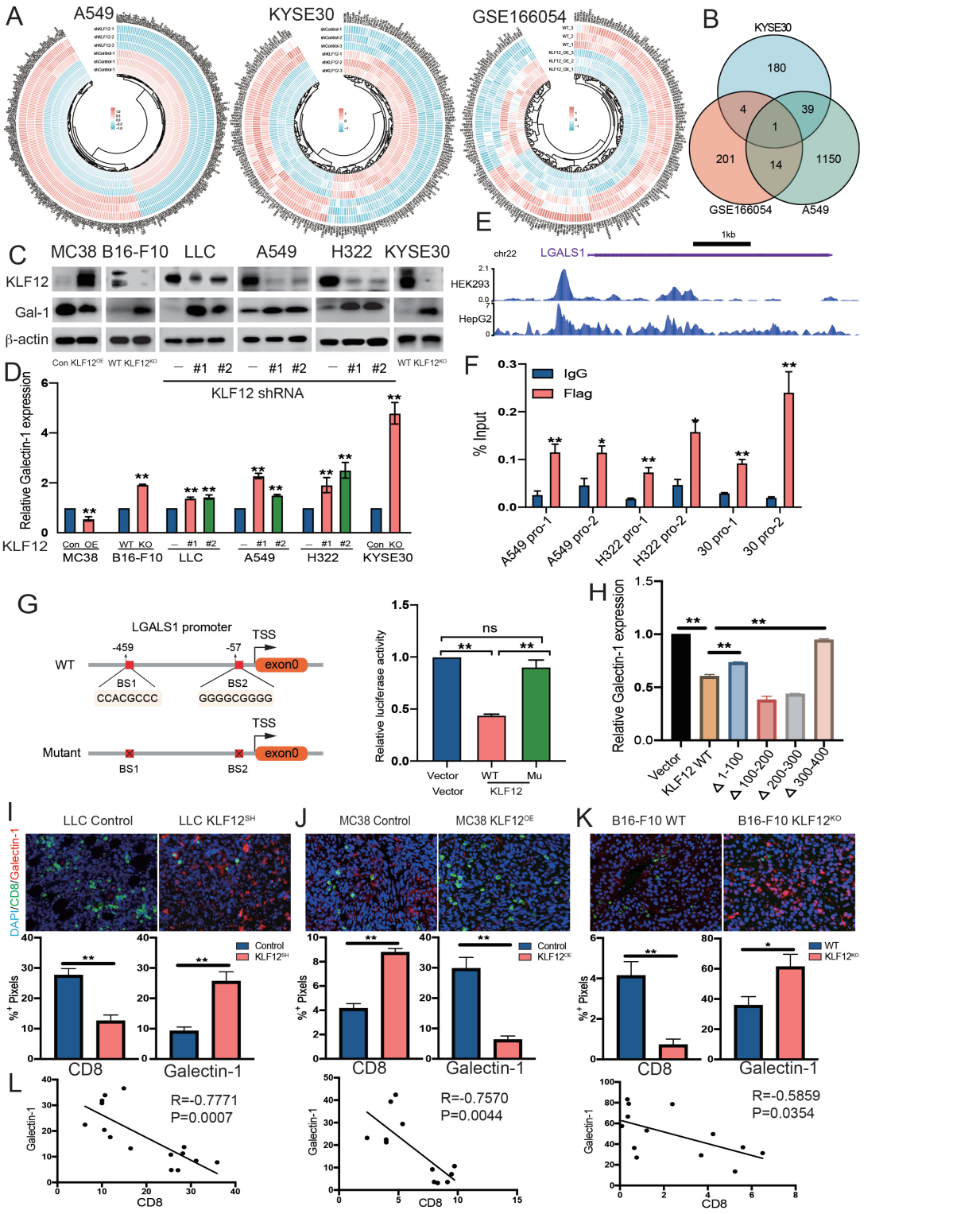

Figure 4 Gal-1 expression was decreased by KLF12. (A) Heat map depicting the expression of DEGs in control, KLF12^{SH} A549, KYSE30, and KLF12 overexpressed mouse cells. (B) Venn diagram analysis of DEGs among comparison groups. (C, D) Altered Gal-1 expression was confirmed via WB (C) and qPCR (D) in human and mouse cell lines. (E) ChIP-seq tracks of KLF12 in HEK293 and HepG2 cells at *lgals1* gene loci. (F) ChIP-qPCR analysis of KLF12 binding to the Gal-1 promoter in A549, H322, and KYSE30 cells. (G) HEK293 cells were transfected with wild-type (WT) or mutant (MU) Gal-1 promoter-luciferase reporter and KLF12 overexpression plasmid for 24 hours and were subsequently assessed via luciferase assays. (H) Gal-1 expression in overexpressed Flag-tagged WT or various truncated KLF12 mutants HEK293 detected using qPCR. (I–K) Representative micrographs of immunofluorescent staining of CD8 (green) and Gal-1 (red) in mice tumor tissues and (L) correlation analysis of their quantification (n=14, 6, 10). DAPI, blue. (Scale bars, 50 µm). ChIP, chromatin immunoprecipitation; DAPI, 4',6-Diamidino-2-phenylindole dihydrochloride; DEG, differentially expressed gene; Gal-1, galectin-1; KLF12, Krüppel-like factor 12; qPCR, quantitative PCR.

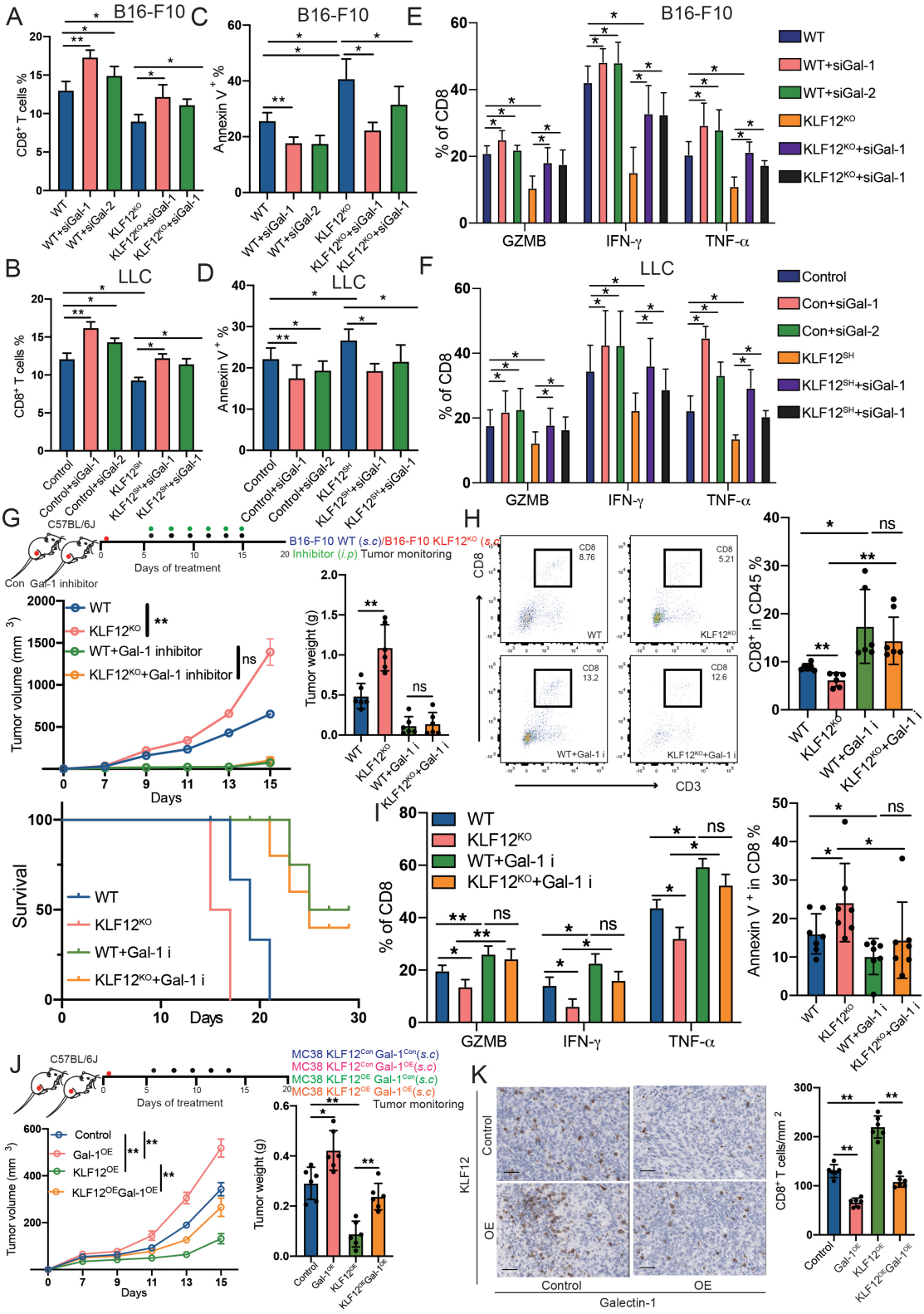

Figure 5 Gal-1 is involved in antitumor CD8$^+$ T-cell responses. (A, B) Percentage of CD8$^+$ T-cell migration. (C, D) Percentage of annexin V$^+$ CD8$^+$ T cell. (E–F) Levels of GZMB, IFN-γ and TNF-α in CD8 T cells, analyzed using FACS. (G) WT and KLF12^{KO} B16-F10-bearing (s.c.) mice received Gal-1 inhibitor or phosphate buffered saline. Tumor growth (n=6) and mice survival (n=6) were then analyzed. (H–I) Percentages of CD8$^+$ T cells (H) and GZMB$^+$, IFN-γ$^+$, TNF-α$^+$, and annexin V$^+$ CD8$^+$ T cells (I) in WT and KLF12^{KO} B16-F10 tumor tissues with or without Gal-1 inhibitor. KLF12 knockdown decreased significantly. (J, K) MC38, KLF12^{OE} MC38, Gal-1^{OE} MC38, and KLF12^{OE} Gal-1^{OE} MC38 tumors volume were monitored (J). Two weeks later, tumor infiltration of CD8$^+$ T cells was detected as in (K) (scale bar, 50 µm, n=5 mice/group). FACS, flow cytometry; GZMB, granzyme B; IFN, interferon; KLF12, i.p., intraperitoneally; KLF12, Krüppel-like factor 12; s.c., subcutaneous; TNF, tumor necrosis factor; WT, wild-type.

figure S6B,C, middle). To determine the effect of Gal-1 on $CD8^+$ T-cell function, we examined the ability of $CD8^+$ T cells to secrete GZMB, IFN-γ, and TNF-α. Gal-1 inhibition reversed the decline in $CD8^+$ T-cell function following KLF12 depletion (figure 5E,F and online supplemental figure S6B,C, right). We also detected the effect of KLF12 and Gal-1 on $CD8^+$ T-cell expansion through BrdU assay and Ki67 staining. Compared with the control, overexpression of KLF12 can promote BrdU and Ki67 expression in $CD8^+$ T cells, while knockdown of KLF12 leads to decreased BrdU and Ki67 expression in $CD8^+$ T cells, and the use of Gal-1 inhibitors reversed the decline $CD8^+$ T-cell expansion following KLF12 depletion. These results showed that KLF12 could promote $CD8^+$ T-cell expansion, and Gal-1 could inhibit $CD8^+$ T-cell expansion (online supplemental figure S6D). Moreover, the Gal-1 inhibitor decreased tumor growth and prolonged survival in mice (figure 5G and online supplemental figure S7A). KLF12 failed to enhance intratumoral $CD8^+$ T-cell accumulation in WT B16F-10 tumors compared with that in $KLF12^{KO}$ B16F-10 tumors following the application of Gal-1 inhibitor (figure 5H and online supplemental figure S7B). Gal-1 inhibitor also improved $CD4^+$ T-cell infiltration (online supplemental figure S7C). In addition, compared with KLF12 deletion alone, simultaneous deletion of KLF12 and Gal-1 inhibitor increased $CD8^+$ T-cell infiltration and function, and reduced apoptosis, as shown by GZMB, IFN-γ, TNF-α, and annexin V expression (figure 5I). We simultaneously developed KLF12 and Gal-1 co-overexpressing MC38 cells, and the results of subcutaneous tumor formation showed that Gal-1 overexpression significantly promoted tumor growth (figure 5J and online supplemental figure S7D) and reduced T-cell infiltration (figure 5K). These results suggest that tumor KLF12 may modulate the immune response and inhibit tumor progression by regulating Gal-1 expression.

KLF12 inhibition impedes the efficacy of anti-PD-1 therapy in cancer

Checkpoint inhibition immunotherapy is one of the most successful strategies for the treatment of several cancers. The increase in the number of immune cells, such as $CD8^+$ T cells, and the expression of PD-1 can improve the efficacy of the anti-PD-1 reaction.[34] We previously found that both the high expression of KLF12 and inhibition of Gal-1 could increase the infiltration of $CD8^+$ T cells and enhance their killing ability in the TME. Here, we analyzed the relationship between KLF12 and Gal-1 and immune checkpoints using the TCGA database and found that KLF12 was positively correlated with most immune checkpoints, whereas Gal-1 was negatively correlated with most immune checkpoints (online supplemental figure S7A). In addition, IHC was performed to identify PD- 1 expression in the TME, and the results showed that $KLF12^{OE}$ triggered the accumulation of $PD\text{-}1^+$ tumor-infiltrating lymphocytes (TILs), and $KLF12^{KO}$ and $KLF12^{SH}$ decreased the number of $PD\text{-}1^+$ cells (online supplemental figure S7B). WT and $KLF12^{KO}$ B16-F10 tumors were used to determine whether KLF12 could enhance anti-PD-1 therapy. We observed that low expression of KLF12 suppressed the immunotherapy effect (figure 6A). The therapeutic efficacy of anti-PD-1 was reduced in mice inoculated with $KLF12^{SH}$ LLC cells compared with those injected with control LLC cells (figure 6B). These results suggested that KLF12 improves the efficacy of anti-PD-1 therapy. To confirm the relationship between KLF12 and Gal-1 and the response to anti-PD-1 treatment, we performed multiplex immunofluorescence in patients with esophageal cancer who received anti-PD-1. KLF12 expression was higher in the anti-PD-1 response group, whereas Gal-1 expression was lower than that in the non-response group. We found that anti-PD-1 responsive tumors tended to have higher overall levels of $CD8^+$ T-cell infiltration and PD-1 expression (figure 6C,D). Similar results were obtained in the NSCLC cohort comprising 12 non-responders and 8 responders (figure 6E,F). Correlation analysis also revealed that KLF12 negatively correlated with Gal-1 and positively correlated with CD8 and PD-1 in the esophageal (figure 6G and online supplemental figure S7C) and NSCLC (figure 6H and online supplemental figure S7D) cohorts treated with anti-PD-1. We observed that patients with high KLF12 and low Gal-1 levels had higher response rates after anti-PD-1 therapy. KLF12 potentiates anti-PD-1 response and KLF12 and Gal-1 were predictors of anti-PD-1 efficacy.

Gal-1 inhibition improves the efficacy of anti-PD-1

Gal-1 promotes tumor progression.[35–37] We queried the TCGA database to determine whether Gal-1 expression was associated with tumor progression and patient prognosis. We found that Gal-1 expression in cancer cells was higher than that adjacent to cancer (online supplemental figure S8A). Kaplan-Meier survival analysis indicated that patients with high Gal-1 expression had a poor prognosis in lung adenocarcinoma (LUAD), lung squamous cell carcinoma (LUSC), colon adenocarcinoma (COAD), and skin cutaneous melanoma (SKCM) (online supplemental figure S8B). To verify the predictive role of Gal-1 in prognosis, 161 lung, 53 esophageal, and 173 colorectal cancers were analyzed. Increased Gal-1 expression was observed in tumor tissues compared with normal tissues (figure 7A–C, left), and Gal-1 was a significant negative prognostic indicator (figure 7A–C, right), and a significant association between Gal-1, lymph node metastasis, and clinical stage (online supplemental figure S8F–G). Moreover, Gal-1 expression was low and CD8 infiltration and PD-1 expression increased in tissues with high KLF12 expression. We observed a significant correlation between these four molecules (figure 7D–F and online supplemental figure S8C–E); based on these results, we speculated that Gal-1 inhibitors improve the therapeutic effect of anti-PD-1. Therefore, we used an anti-PD-1 plus Gal-1 inhibitor in LLC and B16-F10 tumor models. We examined the effect of a combination treatment on tumor growth in B16-F10 and LLC cells by monitoring the tumor volume of mice. We found that the efficacy of the

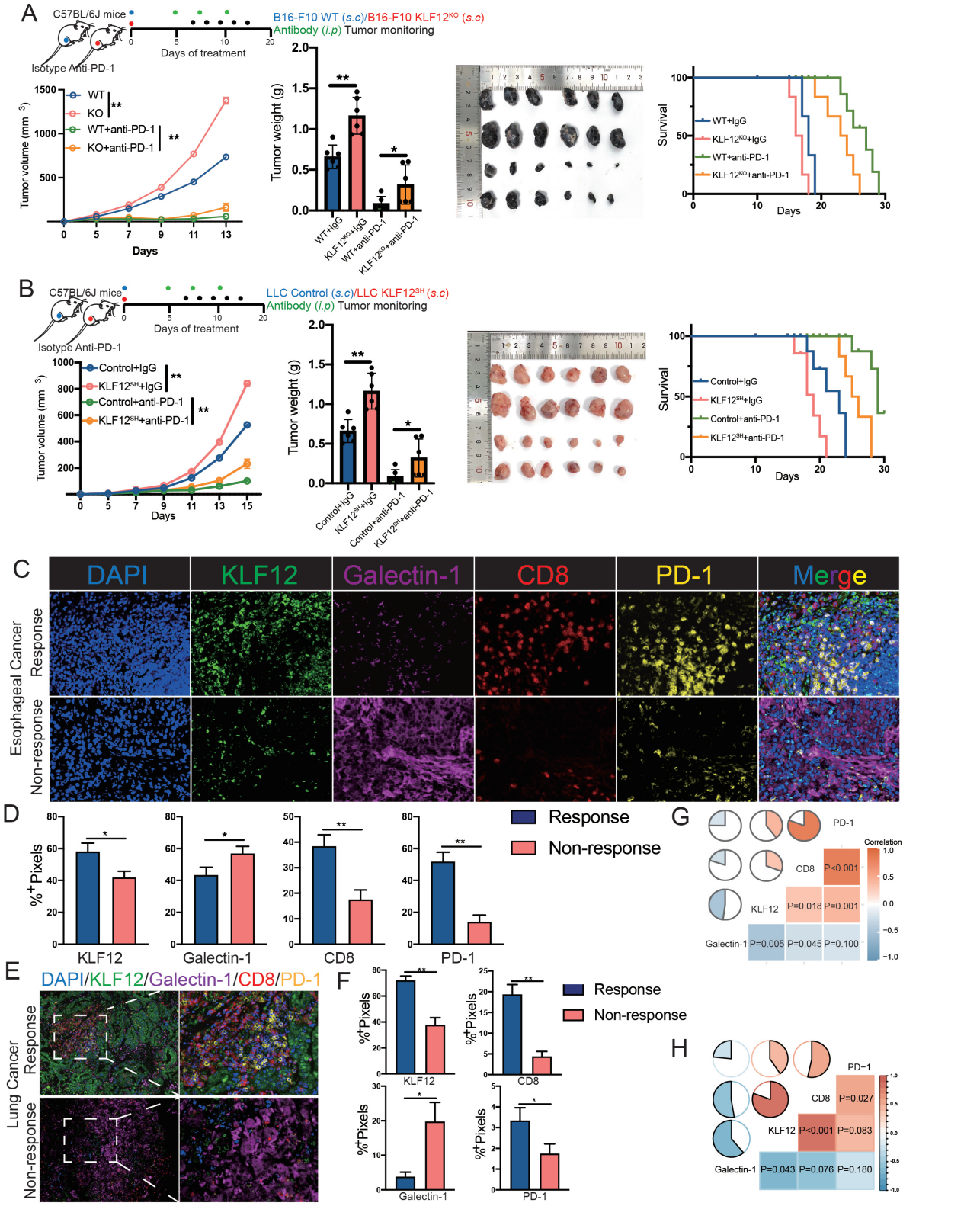

Figure 6 KLF12 enhances the efficacy of anti-PD-1 in different types of cancer. (A) WT and KLF12^{KO} B16-F10-bearing (s.c.) mice received anti-PD-1 or IgG. Tumor growth and mice survival were subsequently analyzed (n=6 mice/group; (B) control and KLF12^{SH} LLC-bearing (s.c.) mice received anti-PD-1 or IgG. Tumor growth and mice survival were subsequently analyzed (n=6 mice/group; (C–F) representative multispectral images from esophageal (C) and lung cancer (E) samples showing DAPI (blue), KLF12 (green), Gal-1 (magenta), CD8 (red), and PD-1 (yellow). The white bars represent 50 µm. Expression of KLF12, Gal-1, CD8, and PD-1 in response and non-response ES (D) and NSCLC (F) samples. (G, H) Correlation matrix of the risk score and four selected genes in ES (G) and NSCLC (H). DAPI, 4',6-Diamidino-2-phenylindole dihydrochloride; ES, esophageal cancer; Gal-1, galectin-1; i.p., intraperitoneally; KLF12, Krüppel-like factor 12; NSCLC, non-small cell lung cancer; PD-1, programmed death-ligand 1; s.c., subcutaneous; WT, wild-type.

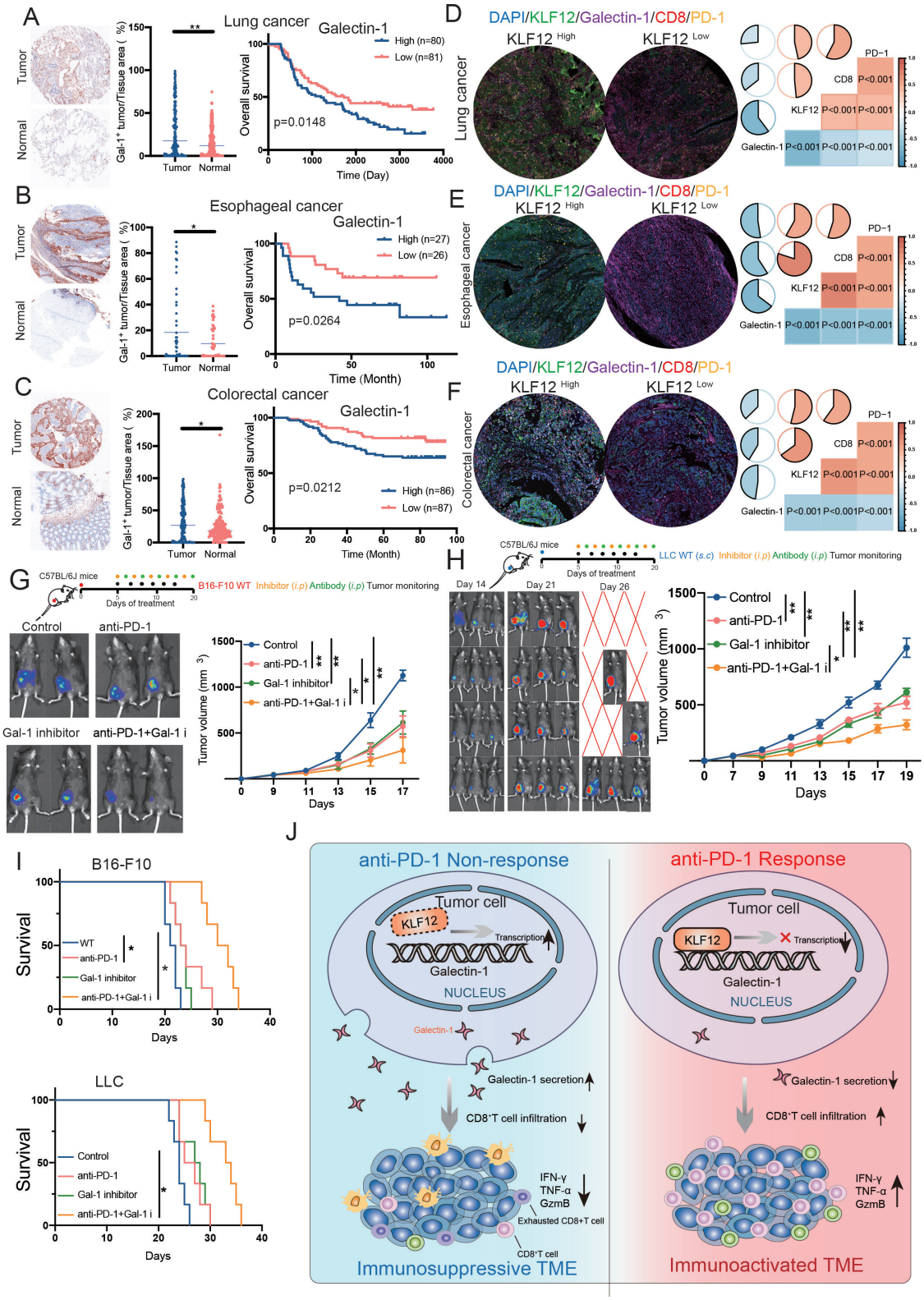

Figure 7 Gal-1 correlates to tumor prognosis and immunotherapy resistance. (A–C) Immunohistochemistry staining of Gal-1. Scale bars, 100 µm. Gal-1 expression in human tumor tissues and paired adjacent normal tissues, and Kaplan-Meier survival curves for lung (A), esophageal (B), and colorectal (C) cancer. (D–F) Correlation between KLF12, Gal-1, CD8, and PD-1 in lung (D), esophageal (E), and colorectal (F) cancer. (G, H) B16-F10 and LLC-tumor-bearing mice received anti-PD-1, Gal-1 inhibitor, or both. Representative bioluminescence images of mice and tumor volume of the B16-F10 (G) and LLC tumor (H). (I) Overall survival of mice. (J) Schematic model for the role of KLF12/Gal-1 modulating antitumor immunity. DAPI, 4',6-Diamidino-2-phenylindole dihydrochloride; Gal-1, galectin-1; GZMB, granzyme B; IFN, interferon; i.p., intraperitoneally; KLF12, Krüppel-like factor 12; PD-1, programmed death-ligand 1; s.c., subcutaneous; TME, tumor microenvironment; TNF, tumor necrosis factor; WT, wild-type.

combination of anti-PD-1 and Gal-1 inhibitor was significantly better than that of therapy alone (figure 7G–I). Collectively, these data indicated that Gal-1 affects human outcomes in several cancer types. In addition, the inhibition of Gal-1 in combination with anti-PD-1 immunotherapy has a favorable effect (figure 7J).

DISCUSSION

Most patients with cancer do not respond to immune checkpoint therapy, and the initial response to immunotherapy eventually leads to drug resistance. Although recent studies have extensively explored the mechanisms of immune resistance to improve treatment outcomes,[38 39] treatment resistance remains a conundrum. The infiltration of immune cells into the TME is closely related to the efficacy of immunotherapy. In patients with tumor, immune responders exhibit a "hot" ("immune-inflammatory") phenotype, characterized by increased T lymphocyte infiltration, whereas non-responders may exhibit a "cold" ("immune-desert") phenotype, characterized by T-cell loss in the tumor parenchyma.[40 41] Based on this rationale, various therapies have been combined with ICI to promote immune recruitment and turn cold tumors into hot tumors. Current research focuses on the interaction between immune cells. Tumor cells play a crucial role in the microenvironment and exert a vital influence on immune cells. In this study, we focused on the interaction between tumor cells and immune cell subsets in the TME, aiming to identify the important factors affecting T-cell infiltration and function to improve immunotherapy responses. In this study, we demonstrated that the decline in KLF12 in tumor cells is an important mechanism for immune escape, leading to resistance to anti-PD-1 therapy. In multiple murine tumor models, the combination of anti-PD-1 and Gal-1 inhibition improved T-cell infiltration, restored T-cell function, and increased the cure rate of tumors.

KLF12 is a transcription factor with a zinc finger domain that extensively regulates gene expression during tumor proliferation and invasion.[11 42] Several studies have detected reduced levels of KLF12 in cancer, which plays a role in tumor metastasis.[43] Unexpectedly, we found that KLF12 is an immunomodulatory molecule that is involved in tumor immunity. We demonstrated a relationship between KLF12 and tumor immunity in multiple mouse tumor models. Thus, we identified tumor KLF12 as a novel mechanism of drug resistance in tumor immunity and immunotherapy. Continued research into the mechanisms of action of KLF12, development and discovery of new targets, and new combination therapies for circumventing drug resistance may provide more effective treatment options for patients with cancer. Despite the evident tumor inhibitory role of tumor KLF12 in vivo in multiple tumor-bearing models, which is associated with immune system regulation, uncovering how KLF12 activates tumor immunity and improves the efficacy of immunotherapy has been challenging.

To develop a more effective combination therapy, we further investigated the specific mechanism of KLF12 regulating TME. By examining the composition of immune cells in the TME, we found that the group with higher KLF12 expression had more infiltration of $CD8^+$ T cells, whereas the other types of immune cells showed no difference. Notably, KLF12 promoted the invasion of $CD8^+$ T cells. KLF12 is a transcription factor that regulates the expression of multiple genes. The results of ChIP-seq and transcriptomic sequencing showed that Gal-1 was a key downstream molecule of KLF12. The ChIP-PCR assay and dual fluorescence reporter experiments suggested that KLF12 could directly bind to the promoter region of Gal-1 and inhibit its expression. We identified a novel mechanism for Gal-1 upregulation in the TME. Thus, we hypothesized that KLF12 mediates its immune-promoting effect on T cells by inhibiting Gal-1.

Gal-1 is a secretory protein that regulates cell signals via its impact on both intracellular and extracellular mechanisms.[44] Gal-1 has extensive influence on tumor progression through glycosylation-dependent or independent mechanisms, which regulate proliferation, immune response, cell cycle progression and apoptosis, induce angiogenesis, inflammation and metastasis.[45 46] As an effective target for cancer therapy and inhibition, Gal-1 has direct anti-proliferative effects on cancer cells and anti-angiogenic effects on tumors.[18 47] Gal-1 expression in classical Hodgkin's lymphoma has been examined revealing a key role of AP-1.[48] In colorectal cancer, Gal-1 is regulated by HIF-1.[49] Gal-1 is a direct transcriptional target of STAT3 in glioblastoma.[33] In human esophageal squamous cell carcinoma, c-Myc binds to Gal-1 promoter regulates its transcription.[50] However, the mechanism of Gal-1 overexpression in other tumor tissues remains elusive. T-cell survival and death are regulated by several signaling mechanisms. Gal-1 plays an important role in tumor immune escape by inducing T-cell apoptosis[51 52] and inhibits T-cell production of the antitumor cytokine IFN-γ.[20 53] Published research has established that Gal-1 regulates T cell by directly binding CD3, CD7, CD29, CD43, and CD45.[52 54–56] Inhibition of Gal-1 can reduce tumor growth, promote T lymphocyte infiltration, and increase IFN-γ production.[47] The rapid development of glycobiology research has accelerated the clinical application of anti-galectin therapy. With our deepening understanding of the role of Gal-1 in cancer, various chemical and biological agents for Gal-1 have been developed for clinical treatment and have achieved good therapeutic effects.[57] However, the treatment effect of complete remission cannot be achieved by using the targeted drug of Gal-1 alone. Interestingly, blocking Gal-1 can enhance the immune stimulation of anti-PD-1 treatment in head and neck squamous cell carcinoma (HNSCC).[23] But this conclusion has not been confirmed and supported by other articles, our study on lung cancer, melanoma, and colorectal cancer also expands the indication for Gal-1 inhibitor. We investigated the effects of tumor KLF12 and Gal-1 on the anti-PD-1 response. We observed that a high

expression of KLF12 had a better immunotherapy effect, and the efficacy of a combination of anti-PD-1 and Gal-1 inhibitor was significantly better than that of therapy alone.

In summary, our findings demonstrated that KLF12 could directly bind to the promoter region of Gal-1 and inhibit its expression. We identified a novel mechanism for Gal-1 upregulation in the TME. And decreased KLF12 and increased Gal-1 expression are associated with the resistance to anti-PD-1 immunotherapy, increased KLF12 expression or the combined use of Gal-1 inhibitors can improve anti-PD-1 response. These findings provide useful mechanistic insights into the antitumor and potential synergistic effects of combining immune checkpoint blockade with a Gal-1 inhibitor in tumors, and the KLF12/Gal-1 axis may serve as a novel therapeutic target.

Acknowledgements All authors would like to acknowledge the efforts of TCGA and GSE166054, GSM2026901, and GSE170637, and thank all the patients analyzed in this study.

Contributors YZ, HZ, CL and JH conceived and designed the study. HZ, CL and JH supervised the study. YZ, CX, ZD, TF and BZ conducted experiments and data analysis. YZ wrote the manuscript. All the authors approved the manuscript. JH is the guarantor for this article.

Funding This work was supported by the National Key R&D Program of China (2021YFF1201300, 2020AAA0109505, YS2021YFF120009), the National Natural Science Foundation of China (82202864, 81972196), the CAMS Innovation Fund for Medical Sciences (CIFMS) (2021-1-I2M-012), and the R&D Program of Beijing Municipal Education commission (KJZD20191002302).

Competing interests None declared.

Patient consent for publication Not applicable.

Ethics approval Not applicable.

Provenance and peer review Not commissioned; externally peer reviewed.

Data availability statement Data are available in a public, open access repository. Data are available upon reasonable request.

ORCID iDs
Chu Xiao http://orcid.org/0000-0002-2985-3440
Jie He http://orcid.org/0000-0003-0327-8852

REFERENCES

1 Hammerbacher J, Snyder A. Informatics for cancer immunotherapy. *Ann Oncol* 2017;28(suppl_12):xii56–73.
2 Ribas A, Wolchok JD. Cancer Immunotherapy using checkpoint blockade. *Science* 2018;359:1350–5.
3 O'Donnell JS, Teng MWL, Smyth MJ. Cancer immunoediting and resistance to T cell-based immunotherapy. *Nat Rev Clin Oncol* 2019;16:151–67.
4 Topalian SL, Hodi FS, Brahmer JR, *et al*. Safety, activity, and immune correlates of anti-PD-1 antibody in cancer. *N Engl J Med* 2012;366:2443–54.
5 Zhou Z, Chen M-J, Luo Y, *et al*. Tumor-intrinsic SIRPA promotes sensitivity to checkpoint inhibition immunotherapy in melanoma. *Cancer Cell* 2022;40:1324–40.
6 Fridman WH, Pagès F, Sautès-Fridman C, *et al*. The immune Contexture in human tumours: impact on clinical outcome. *Nat Rev Cancer* 2012;12:298–306.
7 Zou W. Immunosuppressive networks in the tumour environment and their therapeutic relevance. *Nat Rev Cancer* 2005;5:263–74.
8 Chryplewicz A, Scotton J, Tichet M, *et al*. Cancer cell autophagy, reprogrammed macrophages, and remodeled vasculature in glioblastoma triggers tumor immunity. *Cancer Cell* 2022;40:1111–27.
9 Roth C, Schuierer M, Günther K, *et al*. Genomic structure and DNA binding properties of the human zinc finger transcriptional repressor AP-2Rep (Klf12). *Genomics* 2000;63:384–90.
10 Zhou D, Gu J, Wang Y, *et al*. Long non-coding RNA Neat1 transported by extracellular Vesicles contributes to breast cancer development by sponging microRNA-141-3p and regulating Klf12. *Cell Biosci* 2021;11:68.
11 Liu Y, Wang J, Shou Y, *et al*. Restoring the epigenetically silenced lncRNA Col18A1-As1 represses ccRCC progression by lipid browning via miR-1286/Klf12 axis. *Cell Death Dis* 2022;13:578.
12 He Z, Guo X, Tian S, *et al*. Microrna-137 reduces stemness features of pancreatic cancer cells by targeting Klf12. *J Exp Clin Cancer Res* 2019;38:126.
13 Zhang Q, Wang J, Qiao H, *et al*. Isg15 is downregulated by Klf12 and implicated in maintenance of cancer stem cell-like features in cisplatin-resistant ovarian cancer. *J Cell Mol Med* 2021;25:4395–407.
14 Kim S-H, Park Y-Y, Cho S-N, *et al*. Krüppel-like factor 12 promotes colorectal cancer growth through early growth response protein 1. *PLoS ONE* 2016;11:e0159899.
15 Mao S, Lu Z, Zheng S, *et al*. Exosomal miR-141 promotes tumor angiogenesis via Klf12 in small cell lung cancer. *J Exp Clin Cancer Res* 2020;39:193.
16 Guda MR, Tsung AJ, Asuthkar S, *et al*. Galectin-1 activates carbonic anhydrase IX and modulates glioma metabolism. *Cell Death Dis* 2022;13:574.
17 Tsai Y-T, Li C-Y, Huang Y-H, *et al*. Galectin-1 orchestrates an inflammatory tumor-stroma crosstalk in hepatoma by enhancing Tnfr1 protein stability and signaling in carcinoma-associated fibroblasts. *Oncogene* 2022;41:3011–23.
18 Astorgues-Xerri L, Riveiro ME, Tijeras-Raballand A, *et al*. Unraveling galectin-1 as a novel therapeutic target for cancer. *Cancer Treat Rev* 2014;40:307–19.
19 Derosiers N, Aguilar W, DeGaramo DA, *et al*. Sweet immune checkpoint targets to enhance T cell therapy. *J Immunol* 2022;208:278–85.
20 Rubinstein N, Alvarez M, Zwirner NW, *et al*. Targeted inhibition of Galectin-1 gene expression in tumor cells results in heightened T cell-mediated rejection; A potential mechanism of tumor-immune privilege. *Cancer Cell* 2004;5:241–51.
21 Banh A, Zhang J, Cao H, *et al*. Tumor Galectin-1 mediates tumor growth and metastasis through regulation of T-cell apoptosis. *Cancer Res* 2011;71:4423–31.
22 Cagnoni AJ, Giribaldi ML, Blidner AG, *et al*. Galectin-1 fosters an immunosuppressive Microenvironment in colorectal cancer by Reprogramming Cd8(+) regulatory T cells. *Proc Natl Acad Sci U S A* 2021;118:e2102950118.
23 Nambiar DK, Aguilera T, Cao H, *et al*. Galectin-1-driven T cell exclusion in the tumor Endothelium promotes Immunotherapy resistance. *J Clin Invest* 2019;129:5553–67.
24 Walzel H, Fahmi AA, Eldesouky MA, *et al*. Effects of N-Glycan processing inhibitors on signaling events and induction of apoptosis in Galectin-1-stimulated Jurkat T lymphocytes. *Glycobiology* 2006;16:1262–71.
25 Stillman BN, Hsu DK, Pang M, *et al*. Galectin-3 and Galectin-1 bind distinct cell surface glycoprotein receptors to induce T cell death. *J Immunol* 2006;176:778–89.
26 Femel J, van Hooren L, Herre M, *et al*. Vaccination against Galectin-1 promotes cytotoxic T-cell infiltration in Melanoma and reduces tumor burden. *Cancer Immunol Immunother* 2022;71:2581.
27 Schmitges FW, Radovani E, Najafabadi HS, *et al*. Multiparameter functional diversity of human C2H2 zinc finger proteins. *Genome Res* 2016;26:1742–52.
28 Zhou X, Lowdon RF, Li D, *et al*. Exploring long-range genome interactions using the Washu epigenome browser. *Nat Methods* 2013;10:375–6.
29 Li D, Hsu S, Purushotham D, *et al*. Washu Epigenome Browser update 2019. *Nucleic Acids Res* 2019;47:W158–65.

30 Eisenhauer EA, Therasse P, Bogaerts J, *et al*. New response evaluation criteria in solid tumours: revised RECIST guideline (version 1.1). *European Journal of Cancer* 2009;45:228–47.
31 Stanley P. Galectin-1 pulls the strings on Vegfr2. *Cell* 2014;156:625–6.
32 Jaworski FM, Gentilini LD, Gueron G, *et al*. In vivo Hemin conditioning targets the vascular and immunologic compartments and restrains prostate tumor development. *Clin Cancer Res* 2017;23:5135–48.
33 Sharanek A, Burban A, Hernandez-Corchado A, *et al*. Transcriptional control of brain tumor stem cells by a carbohydrate binding protein. *Cell Rep* 2021;36:109647.
34 Bruni D, Angell HK, Galon J. The immune contexture and immunoscore in cancer prognosis and therapeutic efficacy. *Nat Rev Cancer* 2020;20:662–80.
35 Zhang P, Zhang P, Shi B, *et al*. Galectin-1 overexpression promotes progression and chemoresistance to cisplatin in epithelial ovarian cancer. *Cell Death Dis* 2014;5:e991.
36 Chung L-Y, Tang S-J, Sun G-H, *et al*. Galectin-1 promotes lung cancer progression and chemoresistance by upregulating P38 MAPK, ERK, and cyclooxygenase-2. *Clin Cancer Res* 2012;18:4037–47.
37 Gao J, Wang W. Knockdown of Galectin-1 facilitated cisplatin sensitivity by inhibiting autophagy in neuroblastoma cells. *Chem Biol Interact* 2019;297:S0009-2797(18)30718-X:50–6.:.
38 Vesely MD, Zhang T, Chen L. Resistance mechanisms to anti-PD cancer Immunotherapy. *Annu Rev Immunol* 2022;40:45–74.
39 Huang D, Wang Y, Thompson JW, *et al*. Cancer-cell-derived GABA promotes β-Catenin-mediated tumour growth and immunosuppression. *Nat Cell Biol* 2022;24:230–41.
40 Dammeijer F, van Gulijk M, Mulder EE, *et al*. The PD-1/PD-L1-Checkpoint restrains T cell immunity in tumor-draining lymph nodes. *Cancer Cell* 2020;38:685–700.
41 Zhang J, Huang D, Saw PE, *et al*. Turning cold tumors hot: from molecular mechanisms to clinical applications. *Trends Immunol* 2022;43:523–45.
42 Liu Y, Shi M, He X, *et al*. Lncrna-PACERR induces pro-tumour macrophages via interacting with miR-671-3p and M6A-reader Igf2Bp2 in pancreatic ductal adenocarcinoma. *J Hematol Oncol* 2022;15:52.
43 Godin-Heymann N, Brabetz S, Murillo MM, *et al*. Tumour-suppression function of Klf12 through regulation of anoikis. *Oncogene* 2016;35:3324–34.
44 Thiemann S, Baum LG. Galectins and immune responses-just how do they do those things they do *Annu Rev Immunol* 2016;34:243–64.
45 Liu FT, Rabinovich GA. Galectins as Modulators of tumour progression. *Nat Rev Cancer* 2005;5:29–41.
46 Girotti MR, Salatino M, Dalotto-Moreno T, *et al*. Sweetening the hallmarks of cancer: galectins as multifunctional mediators of tumor progression. *J Exp Med* 2020;217:e20182041.
47 Wu X, Li J, Connolly EM, *et al*. Combined anti-VEGF and anti-CTLA-4 therapy elicits humoral immunity to Galectin-1 which is associated with favorable clinical outcomes. *Cancer Immunol Res* 2017;5:446–54.
48 Juszczynski P, Ouyang J, Monti S, *et al*. The Ap1-dependent secretion of Galectin-1 by reed sternberg cells fosters immune privilege in classical hodgkin lymphoma. *Proc Natl Acad Sci U S A* 2007;104:13134–9.
49 Zhao X-Y, Chen T-T, Xia L, *et al*. Hypoxia inducible Factor-1 mediates expression of Galectin-1: the potential role in migration/invasion of colorectal cancer cells. *Carcinogenesis* 2010;31:1367–75.
50 Yan S, Zhou C, Lou X, *et al*. PTTG overexpression promotes lymph node metastasis in human esophageal squamous cell carcinoma. *Cancer Res* 2009;69:3283–90.
51 Toscano MA, Bianco GA, Ilarregui JM, *et al*. Differential glycosylation of Th1, Th2 and TH-17 Effector cells selectively regulates susceptibility to cell death. *Nat Immunol* 2007;8:825–34.
52 Perillo NL, Pace KE, Seilhamer JJ, *et al*. Apoptosis of T cells mediated by Galectin-1. *Nature* 1995;378:736–9.
53 Croci DO, Cerliani JP, Dalotto-Moreno T, *et al*. Glycosylation-dependent lectin-receptor interactions preserve angiogenesis in anti-VEGF refractory tumors. *Cell* 2014;156:744–58.
54 Camby I, Le Mercier M, Lefranc F, *et al*. Galectin-1: a small protein with major functions. *Glycobiology* 2006;16:137R–157R.
55 Bi S, Earl LA, Jacobs L, *et al*. Structural features of galectin-9 and galectin-1 that determine distinct T cell death pathways. *J Biol Chem* 2008;283:12248–58.
56 Lau LS, Mohammed NBB, Dimitroff CJ. Decoding strategies to evade Immunoregulators Galectin-1, -3, and -9 and their ligands as novel Therapeutics in cancer Immunotherapy. *Int J Mol Sci* 2022;23:15554.
57 Mariño KV, Cagnoni AJ, Croci DO, *et al*. Targeting Galectin-driven regulatory circuits in cancer and fibrosis. *Nat Rev Drug Discov* 2023;22:295–316.